



## OPEN ACCESS

## EDITED BY

Xiaohu Yang,  
Xi'an Jiaotong University, China

## REVIEWED BY

Haowei Yao,  
Zhengzhou University of Light Industry, China  
Zhiyuan Shen,  
Shenyang Jianzhu University, China

## \*CORRESPONDENCE

Jinhai Xu,  
✉ 441560931@qq.com

RECEIVED 27 October 2025

REVISED 05 December 2025

ACCEPTED 08 January 2026

PUBLISHED 24 February 2026

## CITATION

Li H, Xu J, Zhang Z, Li W, Fan Y and Jin Z  
(2026) Study of the hydraulic cavitation  
mechanism and aperture optimization of  
drilling in high-gas coal seams.  
*Front. Earth Sci.* 14:1733210.  
doi: 10.3389/feart.2026.1733210

## COPYRIGHT

© 2026 Li, Xu, Zhang, Li, Fan and Jin. This is  
an open-access article distributed under the  
terms of the [Creative Commons Attribution  
License \(CC BY\)](https://creativecommons.org/licenses/by/4.0/). The use, distribution or  
reproduction in other forums is permitted,  
provided the original author(s) and the  
copyright owner(s) are credited and that the  
original publication in this journal is cited, in  
accordance with accepted academic practice.  
No use, distribution or reproduction is  
permitted which does not comply with  
these terms.

# Study of the hydraulic cavitation mechanism and aperture optimization of drilling in high-gas coal seams

Hongtao Li<sup>1,2</sup>, Jinhai Xu<sup>1\*</sup>, Zelin Zhang<sup>2</sup>, Wenxian Li<sup>2</sup>,  
Yongping Fan<sup>2</sup> and Zhiyong Jin<sup>2</sup>

<sup>1</sup>School of Mines, State Key Laboratory for Fine Exploration and intelligent Development of Coal Resources, China University of Mining & Technology, Xuzhou, Jiangsu, China, <sup>2</sup>Zuoquan Wulinhou Mining Co., Ltd., Shanxi Lu'an Group, Jinzhong, China

To enhance gas pre-extraction efficiency in low-permeability, high-gas coal seams and eliminate the danger of coal and gas outbursts at the Wulihou Coal Mine, this study analyzed the influence of the three stress zones surrounding cavitation holes (employed in alternating cavitation gas extraction technology) on gas extraction, based on the stress distribution characteristics around these holes. Two indices—the pressure relief zone area ratio and the plastic zone area ratio—were proposed to evaluate the pressure relief effect induced by the cavitation process. The effectiveness of cavitation holes for pressure relief and permeability enhancement was investigated using FLAC3D numerical simulation. Results indicate that as the cavitation hole size increases, the area of the associated stress relief zone expands, with its spatial extent best characterized by an exponential function. Similarly, the area of the plastic zone surrounding the cavitation hole also expands and is well-described by a cubic function. Both the pressure relief zone area ratio and the plastic zone area ratio exhibit an initial increase followed by a decrease with increasing cavitation hole radius, reaching their peak values within the radius range of [0.4, 0.5] m. Therefore, the optimal radius for cavitation holes is recommended to be between 0.4 m and 0.5 m. This research provides valuable reference for evaluating the pressure relief and permeability improvement effects, as well as for optimizing the aperture of hydraulic cavitation boreholes in high-gas coal seams.

## KEYWORDS

cavity radius, gas extraction, hydraulic cavitation, soft and low-permeability coal seam, unloading-induced permeability increase

## 1 Introduction

Coal is China's dominant energy source, accounting for approximately 57.7% of China's energy consumption in 2019 (Li, 2014; Lou et al., 2024; Lu et al., 2011). In the process of mine production, coal and gas outbursts and gas explosion accidents often cause heavy casualties and economic losses, which restrict the development of coal mines. Gas extraction is an effective method to eliminate gas accidents

(Zhou et al., 2020; Lou et al., 2025). However, the permeability of coal bodies is typically low, ranging from  $(1-100) \times 10^{-3} \mu\text{m}^2$ , which poses challenges and inefficiencies in gas extraction (Zhang et al., 2023; Chen H et al., 2017; Huang et al., 2014). To enhance gas extraction efficiency effectively, corresponding measures to improve coal seam permeability are essential (Gao et al., 2015; Lu et al., 2017; Chen L et al., 2017). These include  $\text{CO}_2$  or  $\text{N}_2$  gas-phase fracturing (Busch and Gensterblum, 2011; Yang et al., 2022; Zhou et al., 2023; Chen et al., 2020), high-pressure water jet techniques, hydraulic fracturing, and hydraulic slotting, among others (Kong et al., 2016; He et al., 2021; Zhang et al., 2017; Liu et al., 2025; Zhang H et al., 2019). In engineering applications, the low-permeability characteristic of Chinese coal seams means gas drainage using these technologies still falls short of meeting actual safe production requirements (Gao et al., 2015; Li et al., 2024; Li et al., 2025).

Zhang et al. (2017) proposed a novel in-seam borehole hydraulic flushing (ISBHF) technology for gas extraction. The consistency between field test results and simulation outcomes validated the reliability of the corresponding numerical model. After applying this new technology, the number of gas extraction boreholes at the heading face decreased by 50%, while the gas extraction concentration and flow rate increased by 10-fold and 6-fold, respectively. Consequently, the gas extraction duration was shortened by 65%, and the monthly excavation length of coal mine roadways doubled. For structural coal seams, Zhang R et al. (2019) conducted research on bedding hydraulic cavitation to strengthen gas drainage. The results indicated that this technology reduced the number of boreholes by 66.7% and increased the gas extraction rate and concentration by 1.33 times and 3 times, respectively, demonstrating significant advantages over traditional extraction methods.

Beyond hydraulic flushing and cavitation technologies, Lin et al. (2015) developed a cross-borehole hydraulic slotting technique. Field application data showed that after half a month of gas extraction, the average gas extraction concentration of slotted boreholes reached 26%, compared to only 7% for conventional boreholes—meaning the concentration of slotted boreholes was approximately 3.7 times that of conventional ones, highlighting the remarkable effectiveness of slotting technology in improving extraction concentration. Zhang H et al. (2019) presented a hydraulic-flushing gas drainage technology. This technology efficiently flushed out more tectonic coal from thick coal seams, and the large-diameter cavities formed in the tectonic coal sub-layers significantly expanded the scope of stress relief and permeability enhancement, thereby remarkably improving gas extraction efficiency. To address the core demands of technological optimization and construction cost reduction, Chen et al. (2020) established a multi-physical coupling model. Through this model, they determined the optimal spacing of hydraulic flushing boreholes (HFB), providing precise parameter support for field tests and filling the gap in quantitative design within this field. However, existing hydraulic enhanced extraction technologies all have obvious limitations, a consensus widely recognized by numerous scholars (Li et al., 2023; Liu et al., 2023; Wang et al., 2021). For instance, hydraulic slotting technology exhibits poor sustainability in permeability enhancement effects. Under high *in situ* stress conditions, the fractures generated by slotting are prone to closure,

leading to a rapid decline in extraction efficiency. Hydraulic fracturing technology, on the other hand, tends to cause local stress concentration in coal masses, which in turn restricts the permeability improvement effect. More critically, both technologies demonstrate poor performance in gas extraction from soft tectonic coal seams. Soft tectonic coal inherently has low strength and disorganized fracture development. Fractures from hydraulic slotting are liable to collapse and close, while hydraulic fracturing may result in overall coal fragmentation that clogs boreholes. This has become a key bottleneck limiting gas control in soft coal seams.

In contrast, borehole hydraulic cavitation has emerged as an innovative pressure relief and permeability enhancement technology, attracting growing attention and extensive research in recent years. The core process of this technology involves three steps: first, drilling conventional boreholes into the coal seam; second, fracturing the coal surrounding the boreholes using high-pressure water jets; and finally, flushing the fragmented coal out of the boreholes to form large-diameter cavities. Compared with competing technologies such as hydraulic slotting and fracturing, its unique advantage lies in achieving long-term stress relief by forming physical cavities rather than relying on fracture structures that are prone to closure. This provides a novel solution to the challenges of gas extraction in soft tectonic coal seams.

Gas cavitation plays a crucial role in the safe and efficient extraction of coalbed methane. Although previous studies have predominantly focused on seepage characteristics, gas cavitation exerts a significant impact on coal mass by altering its stress distribution: through stress relief and concentration effects, this stress change promotes gas desorption from coal matrix pores, increasing coal permeability, and thereby achieves effective gas extraction. Meanwhile, gas cavitation damages the coal surrounding the cavitation hole, leading to the formation of a plastic zone in the affected area. Notably, gas cavitation disrupts the original stress balance of the coal mass, resulting in the formation of a two-zone annular structure within the coal, which is composed of a stress concentration zone and an original stress zone. As the core disturbed region, the stress concentration zone undergoes the redistribution of radial and tangential stresses, accompanied by corresponding variations in coal permeability, and can be further subdivided into two sub-zones. In the fluidized zone, tangential compressive stress drives the opening of coal fractures, leading to a sharp increase in permeability; in the compaction zone, radial compressive stress dominates the coal compaction process, resulting in a temporary reduction in permeability. In contrast, the original stress zone remains in an undisturbed state, with its physical-mechanical properties and seepage characteristics maintaining their initial conditions. Numerical simulations have been conducted to analyze the stress distribution around the cavitation hole and the formation characteristics of the plastic zone. Relevant indicators for evaluating the effectiveness of gas cavitation have been proposed based on field practice, which provide a solid theoretical foundation for the practical application of gas cavitation technology in coalbed methane extraction.

Existing research has not yet clearly studied the mechanism of borehole hydraulic cavitation. Therefore, based on the redistribution of coal stress caused by the excavation of the hole, this article attempts to explain the mechanism of pressure relief and permeability enhancement of the hole from the perspective of

stress. In this article, based on the simulation of engineering practice, limited by the field parameters, only simplified models are used instead of complex models. The innovation is that it is not limited to the conventional gas seepage analysis, but instead offers a new way to analyze the stress change and coal damage in the process of gas cavitation from the mechanical failure mechanism.

Initially, the mechanism of the distressed zone and permeability increase is examined based on the stress distribution law surrounding the cavitation hole. Subsequently, the finite-difference FLAC3D numerical analysis software is utilized in the context of the gas extraction project at the Wulihou Coal Mine in Shanxi, China, to investigate the optimal radius of the cavitation hole. This investigation is conducted by comparing and analyzing variations in the area of the pressure relief zone, the pressure relief area ratio, the plastic zone area, and the plastic zone area ratio for different cavitation hole radii. On this basis, combined with practical engineering, a set of quantitative indicators has been carefully established to accurately evaluate the effect of gas cavitation, injecting new vitality into engineering practice.

## 2 Project overview and engineering geological condition

The Wulihou Coal Mine is situated in Zuoquan County, Shanxi Province. The coal seam has a thickness of approximately 6 m, with an absolute gas outflow of approximately 18 cubic meters per minute and a relative gas outflow of 11 cubic meters per ton, indicating it is a high-gas mine. The maximum principal stress of the lower coal group in Wulihou Coal Mine is horizontal stress, with an average value of 18.5 MPa and a direction angle of N31.65 E ~ N36.53 E; the minimum principal stress is still horizontal stress, with an average value of 10.5 MPa and a direction angle of N121.32 E ~ N125.32 E; the intermediate principal stress is vertical stress, with an average value of 11.5 MPa and a direction angle of N214.95° E ~ N219.83° E. The lower coal seam has a large dip angle, and the strength of the roof and floor mudstone and coal body is small; they are unstable rock strata. Furthermore, the coal seams exhibit limited permeability and diminished compressive strength, complicating gas extraction and heightening the associated risks of coal and gas outbursts.

To guarantee the secure excavation of the belt highway and the track roadway, alternating cavitation technology is employed for gas extraction, as seen in Figure 1. The technical principle is as follows: first, ordinary boreholes are drilled into the coal seam in the belt bottom drainage roadway, subsequently employing high-pressure water to generate current as the energy source to construct a series of cylindrical cave-building chambers within the coal seam. This causes the coal body to unload and increase permeability, thereby facilitating the extraction of coal seam gas. To increase production efficiency and decrease costs, the interval is alternately utilized to position standard drilling holes and cavitation holes. Specifically, a row of acupuncture holes is situated between two rows of standard drilling. However, existing research is insufficient to understand the pressure relief and permeability enhancement effects around the cavitation hole in the coal body. The radius (R) of the cavitation hole may influence the coal unloading and permeability increase, necessitating more investigation.

## 3 Mechanism of pressure relief and permeability enhancement by cavitation holes

The primary coal structure is composed of pores, cracks, coal matrix blocks, and gas, as shown in Figure 2. It is assumed that the coal matrix, pores, cracks, and gas are subjected to the original rock stress ( $\sigma_1, \sigma_2, \sigma_3$ ) before the cave is formed; that is, in the original rock stress state. Then the coal body is caved, the original rock stress balance of the coal body is broken, and the coal body stress is redistributed around the cavitation. After the stress equilibrates, three zones will be formed around the cavitation hole: a stress-decreasing zone (referred to as the stress-relaxation area), the stress concentration zone, and the initial stress area. Within the stress-decreasing zone (the pressure relief shown in Figure 2), the coal body expands the acupuncture points around the cavitation hole, driving the pores and cracks to deform. The pores and cracks also expand under the effect of the gas pressure (such as the gas pressure in Figure 2) inside the hole, propagating the pores and cracks, which leads to an increase in the permeability of the coal body and a decrease in the pressure of the reservoir. As a result of the changes, the gas in the coal body desorbs, diffuses, and seeps into the cavitation. When the stress exceeds the strength limit of the coal body in the stress concentration area, the coal matrix block around the cavitation hole is damaged, and new cracks sprout and connect with the original pores and cracks, which increases the permeability of the coal body. The gas in the coal body diffuses and seeps into the cavitation hole. Within the primary rock stress zone area, the coal body is not affected by the disturbance of the cavitation hole, and it has no effect on the gas in the coal body.

The above analysis shows that the essence of pressure relief is to form a stress reduction zone and a stress concentration area around the cavitation hole, which causes internal changes in the coal body and increases the permeability of the coal body. For this reason, the issue will be analyzed from the perspective of stress distribution. It is assumed that the coal rock mass, overburden rock, and floor are isotropic linear elastic bodies (Ma et al., 2023; Xue et al., 2013). There is an excavation in the infinite elastic body to create acupuncture holes, simplifying the space problem into a plane strain problem. The force diagram of the cavitation hole is shown in Figure 3. The vertical and horizontal original rock stresses are  $p$  and  $q$ , respectively; the radius of the cavitation hole is  $a$ ; the angle of horizontal axis from the horizontal  $t$  to the right to the right time to the unit body is  $\theta$ ; the radial stress is  $\sigma_r$ , the ring stress is  $\sigma_\theta$ , the shear stress is  $\tau_{r\theta}$ , and the side pressure coefficient  $k = p/q$ . The stress on the cavitation hole is the same as that on the horizontal to the right horizontal axis. According to the theory of elasticity, the stresses acting on any tiny cell are (Equation 1).

$$\left. \begin{aligned} \sigma_r &= \frac{1}{2}p(1+k)\left(1 - \frac{a^2}{r^2}\right) - \frac{1}{2}p(1-k)\left(1 - 4\frac{a^2}{r^2} + 3\frac{a^4}{r^4}\right)\cos 2\theta \\ \sigma_\theta &= \frac{1}{2}p(1+k)\left(1 + \frac{a^2}{r^2}\right) + \frac{1}{2}p(1-k)\left(1 + 3\frac{a^4}{r^4}\right)\cos 2\theta \\ \tau_{r\theta} &= \frac{1}{2}p(1-k)\left(1 + 2\frac{a^2}{r^2} - 3\frac{a^4}{r^4}\right)\sin 2\theta \end{aligned} \right\} \quad (1)$$

Based on the vertical stress of the primary stress state on most global coal bodies, the vertical stress of the original rock stress is

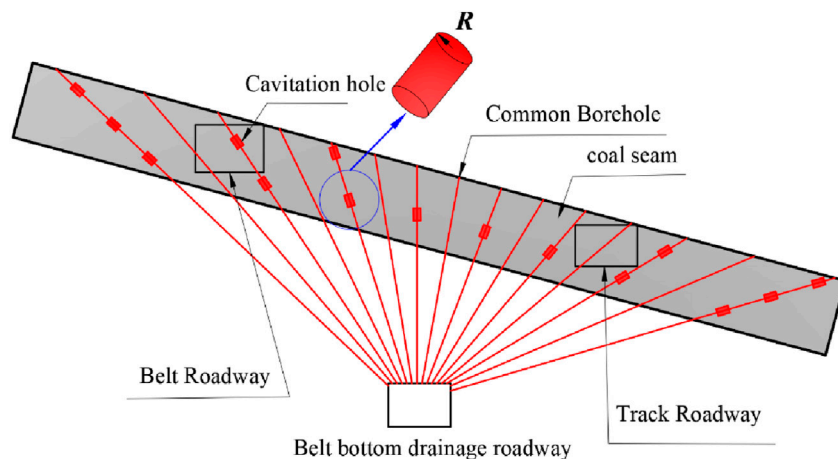


FIGURE 1 Gas extraction schematic diagram of interval alternating cavitation hole-making technology.

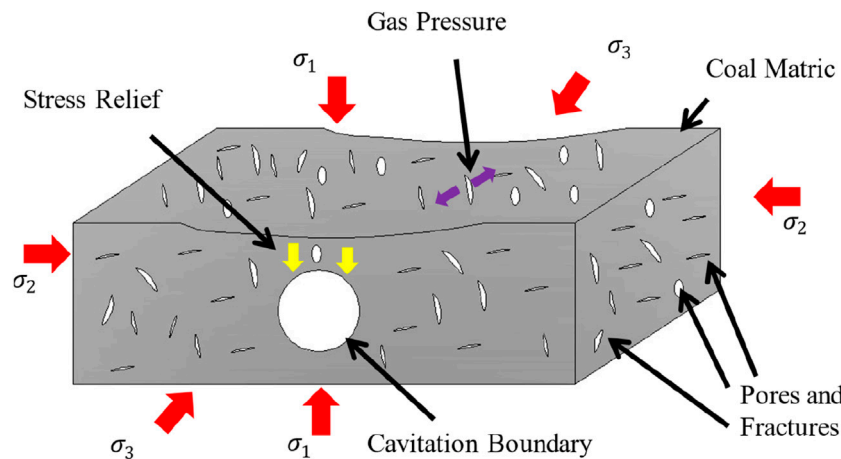


FIGURE 2 Gas extraction schematic diagram.

greater than the horizontal stress, that is,  $k < 1$ . The distribution of cutting stress  $\sigma_\theta$  along the periphery of the hole is shown in Figure 3. The shape of the circular stress distribution curve is related to the value of  $K$ . This curve shape has a value of  $k < 1$ . If  $k < \frac{1}{3}$ , the top (B-B line direction) of the cavitation hole will occur. According to the principle of pressure as “+” and “-” according to rock mechanics, the ring stress distribution curve at the top will be moved. The shape of the acupoint is roughly similar. Therefore, in order not to lose the general nature, the shape of the hoop stress  $\sigma_\theta$  distribution curve in Figure 4 is analyzed.

Figure 4 shows that the hoop stress  $\sigma_\theta$  around the periphery of the cavitation hole has a stress reduction in the direction of the B-B line; that is, it is the stress of the force release or decompression effect. Therefore, it is proposed to analyze the decompression effect of the cavitation hole in the B-B line by the hoop stress in the B-B line direction  $\sigma_\theta$ . In addition, in order to quantify the scope of influence of the decompression effect, the decompression area

ratio is used as a judgment index, which is calculated by the following formula:

$$\eta_s = \frac{S_r}{S}, \tag{2}$$

where  $\eta_s$  denotes the pressure relief area ratio;  $S_r$  represents the area where the hoop stress  $\sigma_\theta$  is diminished following cavitation;  $S$  signifies the area of the cavitation hole.

The hoop stress around the cavitation hole is  $\sigma_\theta$ . There is an increase in stress in the direction of the A-A line; that is, it is a stress concentration, and the stress should be the force concentration that will lead to shear damage of the coal matrix, sprouting new cracks, and increasing the permeability of the coal body. In order to quantify the scope of influence of the increased permeability of the coal body due to the stress concentration, the area ratio of the plastic zone is used as a judgment index, and its calculation formula is as follows:

$$\eta_p = \frac{S_{FP}}{S}, \tag{3}$$

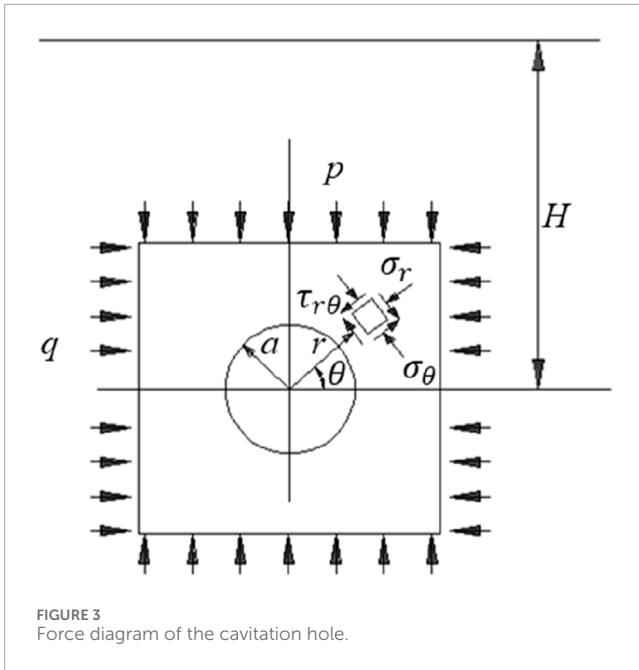


FIGURE 3 Force diagram of the cavitation hole.

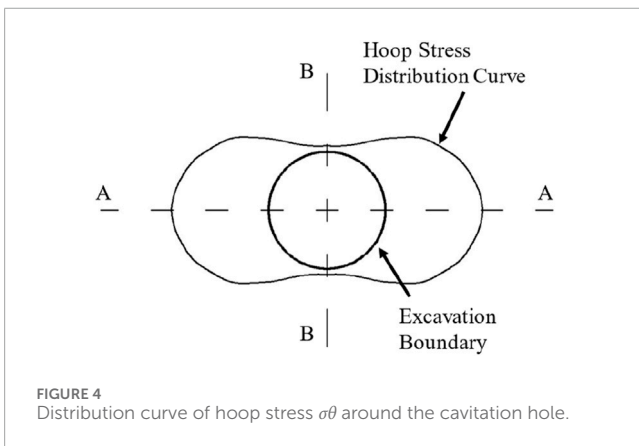


FIGURE 4 Distribution curve of hoop stress  $\sigma_\theta$  around the cavitation hole.

where  $\eta_p$  denotes the plastic zone area ratio;  $S_{FP}$  represents the plastic zone area after cavitation.

## 4 Numerical simulation

### 4.1 Model building

To analyze the effect of unloading pressure and increasing penetration of different cavitation hole diameters, FLAC3D was utilized to create a three-dimensional numerical grid model, as illustrated in Figure 5. The dimensions of the model are 12 m × 10 m × 6 m, with a stress boundary condition applied at the top and a displacement boundary condition at the bottom, front, back, left, and right sides. The coal body utilizes the Moore–Cullen model, and its mechanical parameters are presented in Table 1.

The numerical simulation methodology is delineated as follows: establish the cavitation hole radii at 0.3 m, 0.4 m, 0.5 m, 0.6 m, and 0.7 m, respectively, to investigate the effects of varying cavitation

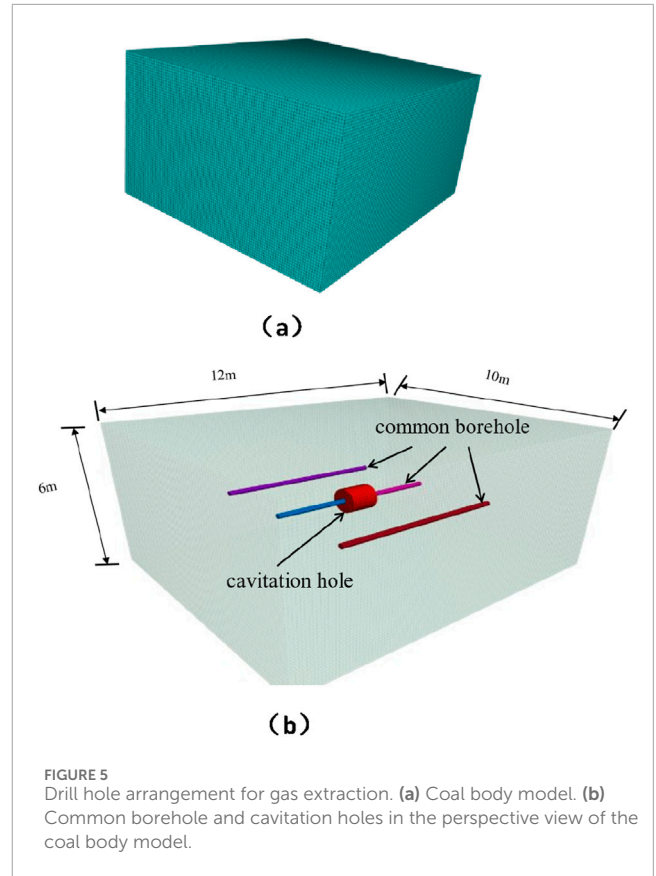


FIGURE 5 Drill hole arrangement for gas extraction. (a) Coal body model. (b) Common borehole and cavitation holes in the perspective view of the coal body model.

TABLE 1 Mechanical parameters of the coal body (Wang et al., 2024; Guo et al., 2023).

$\rho/(\text{kg} \cdot \text{m}^{-3})$	$K/\text{GPa}$	$G/\text{GPa}$	$\varphi/(^{\circ})$	$C_m/\text{MPa}$	$\sigma_t/\text{MPa}$
1410	2.0	0.88	20	0.5	0.2

$\rho$ , density;  $K$ , bulk modulus;  $G$ , shear modulus;  $\varphi$ , friction angle;  $C_m$ , cohesion;  $\sigma_t$ , tensile strength.

hole diameters on the plastic zone, maximum principal stress, and shear strain increment of the surrounding coal body. The distance between the cavitation hole and the standard drill holes is 3 m, and the radius of the standard drill holes is 0.1 m.

When the cavitation hole has a radius of 0.7 m, the top and bottom boundaries are 3 m from the hole’s center, approximately 4.29 times the radius. For the numerical model, the boundary extent shall be specified as six times the radius, pursuant to Equations 5–8 (Liu and Yu, 2012; Xu, 2016). Beyond this range, rock mass variation is approximately 3%, which is negligible. In this case, with a 4.29× radius boundary, the rock mass variation is approximately 5%, still within an acceptable range. This choice minimizes the influence of external rock masses while avoiding a significant increase in grid count and computational load, thus balancing resource use and meeting engineering analysis requirements.

$$\sigma_r = \gamma H_c \left( 1 - \frac{r_0^2}{r^2} \right), \tag{4}$$

$$\sigma_{\theta} = \gamma H_c \left( 1 + \frac{r_0^2}{r^2} \right), \quad (5)$$

$$\tau_{r\theta} = 0, \quad (6)$$

$$u = \frac{\gamma H_c r_0^2}{2Gr}, \quad (7)$$

$$v = 0. \quad (8)$$

In this study, the radius of conventional boreholes is 0.1 m, so the mesh size is set to 0.1 m during modeling, resulting in a mesh count of 278,414. Expanding the boundary would significantly increase the mesh count. For these reasons, the current model boundary is selected.

## 4.2 Analysis of the pressure relief effects of the cavitation hole

### 4.2.1 Stress relief zone analysis

The distribution of maximum principal stresses for different radii of cavitation holes is shown in Figure 6, where the negative numbers indicate rock mass compression. Figure 6a shows that when the radius of the cavitation hole is 0.3 m, the minimum value of the maximum principal stress at the top of the cavitation hole is 1.28 MPa. Compared with the stress in the original rock of 2.39 MPa, it is reduced by 1.11 MPa, and the maximum stress-release rate is 46%. Figure 6b shows that when the radius of the cavitation hole is 0.4 m, the stress-release area in the vertical direction of the cavitation hole is in the shape of a flat long ellipse, and its area is larger than that of the cavitation hole with a radius of 0.3 m, while the stress concentration area in the horizontal direction is in the shape of a circle, and its area is larger than that of the cavitation hole with a radius of 0.3 m. The minimum value of the maximum principal stress at the top of the cavitation hole is 1.05 MPa, which is 1.34 MPa less than the original rock stress, and the maximum stress-release rate is 56%. Figure 6c shows that when the radius of the cavitation hole is 0.5 m, the stress-release area in the vertical direction of the cavitation hole is in the shape of a long flat ellipse, and its area is larger than that of the cavitation hole with a radius of 0.4 m, while the stress concentration area in the horizontal direction is in the shape of a goldfish, and its area is larger than that of the cavitation hole with a radius of 0.4 m. The minimum value of the maximum principal stress at the top of the cavitation hole is 0.876 MPa, which is 1.11 MPa less than the original rock stress, and the maximum stress-release rate is 63%. Figure 6d shows that when the radius of the cavitation hole is 0.6 m, the stress relief area in the vertical direction of the cavitation hole is in the shape of a long flat ellipse, and its area is larger than that of the cavitation hole. The radius of the cavitation hole is 0.5 m larger, and the stress concentration area in the horizontal direction is in the shape of a goldfish, and its area is half that of the cavitation hole. The diameter of 0.5 m is larger. The minimum value of the maximum principal stress at the top of the cavitation hole is 0.849 MPa, which is 1.54 MPa less than the original rock stress, and the maximum stress-release rate is 64%. Figure 6e shows that when the radius of the cavitation hole is 0.7 m, the stress relief area in the vertical direction of the cavitation hole is

in the shape of a long flat ellipse, and its area is larger than that of the cavitation hole with a radius of 0.7 m. When the radius is 0.6 m, the stress relief area decreases, whereas the horizontal stress-concentration zone exhibits a goldfish-like shape, with an area larger than that corresponding to a cavitation hole radius of 0.6 mm. The minimum value of the maximum principal stress at the top of the cavitation hole is 0.77 MPa, which is 1.62 MPa less than the original rock stress, and the maximum stress-release rate is 68%.

From the shape of the principal stress distribution, when the radius of the cavitation hole changes from 0.3 m to 0.7 m, the stress-release area in the vertical direction of the cavitation hole is flattened with an elongated ellipse shape. However, the stress concentration area in the horizontal direction varies. When the radius of the cavitation hole is 0.3 m or 0.4 m, the stress concentration area assumes a circular shape. When the diameter of the cavitation hole measures 0.5 m, 0.6 m, or 0.7 m, the stress concentration region in the horizontal axis exhibits a goldfish-like morphology. As the radius expands, the zones of stress release and horizontal stress concentration in the vertical direction progressively enlarge.

Figures 6a–e show that, compared to the stress in the original rock, the maximum principal stress in the vertical direction adjacent to the cavitation hole diminishes, while the maximum principal stress in the horizontal direction escalates. As the hole diameter increases, the maximum principal stress in the vertical direction near the cavitation hole continues to decrease significantly, resulting in an expanding stress-release area. The reason is that as the radius of the cavitation cavity increases, the disruption to the coal body intensifies, allowing for greater expansion of the coal body and thus enlarging the stress-release region, so facilitating gas seepage.

The area of the pressure relief zone corresponding to the radius of the cavitation hole is extracted, and a plot of the area of the pressure relief zone against the radius of the cavitation hole is illustrated in Figure 7, which shows that the area of the pressure relief zone progressively enlarges with the radius of the cavitation hole. When the radius of the cavitation hole is  $\geq 0.4$  m, the increase is approximately linear, suggesting that the radius of the cavitation hole significantly influences the area of the pressure relief zone.

To better describe the relationship between the area of the pressure relief zone and the radius of the cavitation hole, two reasonable fitting model assumptions are proposed for the variation curve of the pressure relief zone area with the cavitation hole radius. Two more reasonable fitting model assumptions can be made for the curves of the radius change plots (Equations 9–12):

1. Parabolic model. The curve of the model is

$$S_{r1} = a_3 R^2 + b_3 R + c_3, \quad (9)$$

where  $a_3$ ,  $b_3$ , and  $c_3$  are parameters to be determined in relation to the area of the pressure relief zone.

2. Exponential function model. The curve of the model is

$$S_{r2} = -a_4 b_4^R + c_4, \quad (10)$$

where  $a_4$ ,  $b_4$ , and  $c_4$  are parameters to be determined with respect to the area of the pressure relief zone.

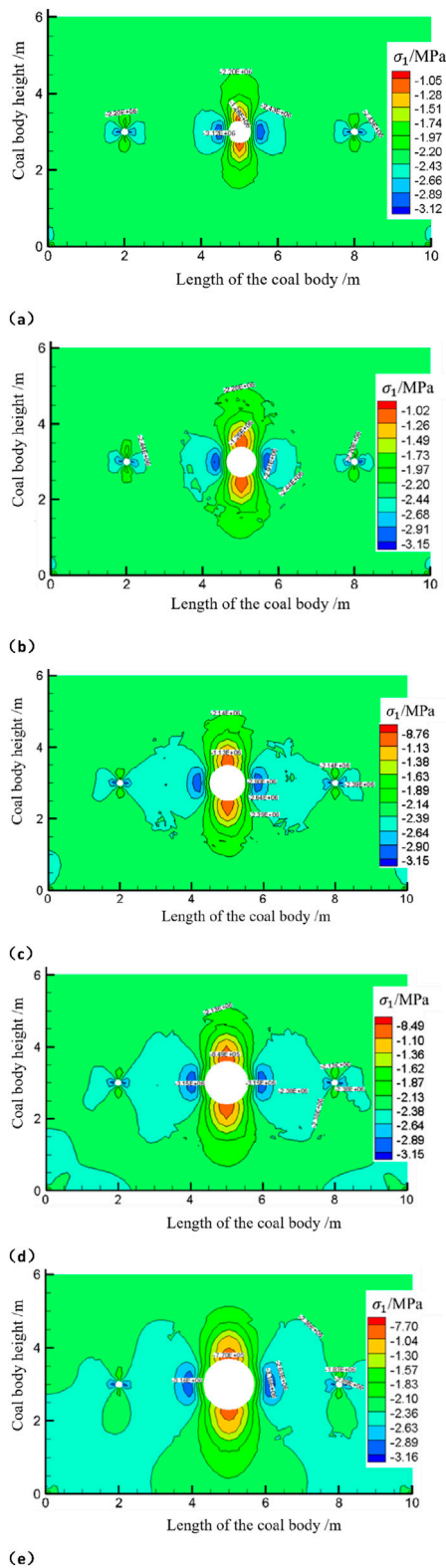


FIGURE 6 Distribution of maximum principal stresses for different radii of cavitation holes: (a) 0.3 m, (b) 0.4 m, (c) 0.5 m, (d) 0.6 m, and (e) 0.7 m.

Based on the extracted values for the radius of the cavitation hole and the area of the pressure relief zone, the fitted curves are obtained, respectively,

$$S_{r1} = -11.9R^2 + 23.2R - 5.2, \tag{11}$$

$$S_{r2} = 1.4 - 15 \times 0.1^R. \tag{12}$$

The coefficients of determination of the fit are, respectively,  $R_{r1}^2 = 0.9920$ ;  $R_{r2}^2 = 0.9942$ .

The above analysis shows that the relationship between the area of the pressure relief zone of the cavitation hole and the radius of the cavitation hole is better fitted by the exponential function model, and the exponential function model can better describe the change of the area of the pressure relief zone of the cavitation hole with the change of the radius of the cavitation hole.

### 4.2.2 Plastic zone analysis

Tensile failure occurs when the tensile stress  $\sigma$  exceeds the tensile strength  $\sigma_t$  of coal, while shear failure occurs when the shear stress  $\tau$  exceeds the shear strength  $\tau_s$  of coal. This kind of strength failure can be intuitively characterized by the distribution characteristics of the plastic zone under different cavitation hole radii, where “none” indicates no yielding, “shear” indicates shear yielding, “tension” indicates tensile yielding, “n” indicates entering yielding at the current step, and “p” indicates entering yielding at the previous step. The core value of this figure lies in clearly presenting the entire process of coal fracture initiation and propagation dominated by tangential stress, and the difference in tangential pressure distribution directly determines the range, morphology, and failure type of fracture opening.

Figure 8a shows that the top and bottom of the cavitation hole exhibit tensile failure characteristics, while the two sides show shear failure. The essence of this phenomenon is the uneven distribution of tangential stress at different positions around the hole: at the top and bottom of the hole, tangential tensile stress dominates. When this stress exceeds the tensile strength  $\sigma_t$  of coal, it directly drives the opening and extension of primary micro-fractures, forming tensile failure zones. On both sides of the hole, tangential compressive stress interacts with radial stress to generate shear stress, triggering the development of shear fractures. Although tangential compressive stress does not directly lead to fracture opening at this time, it provides mechanical conditions for the formation of shear fractures by changing the stress-field distribution. Note that the range of the plastic zone under this radius is relatively small, indicating that the influence depth of tangential stress is limited and the degree of fracture opening is weak, which is highly consistent with the subsequent result that the stress-release rate is only 46%.

A comparison of Figures 8a,b with the increase in cavitation hole radius shows that the plastic zone around the hole expands significantly, and the plastic zone near ordinary boreholes also increases synchronously. The top of the cavitation hole changes from simple tensile failure to combined tension-shear failure, while the two sides are still dominated by shear failure. The core driving

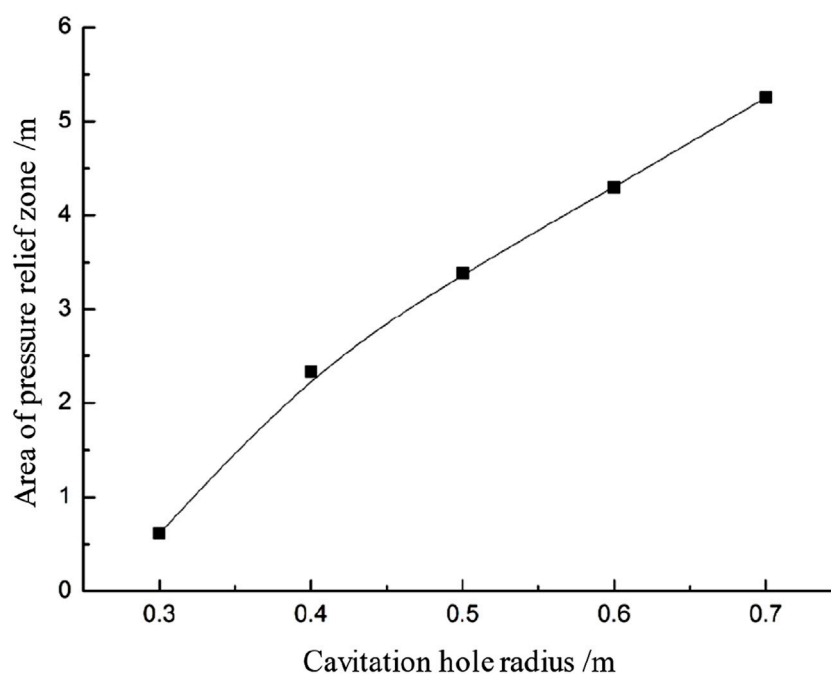


FIGURE 7  
Graph of the variation of the area of the pressure relief zone with the radius of the cavitation hole.

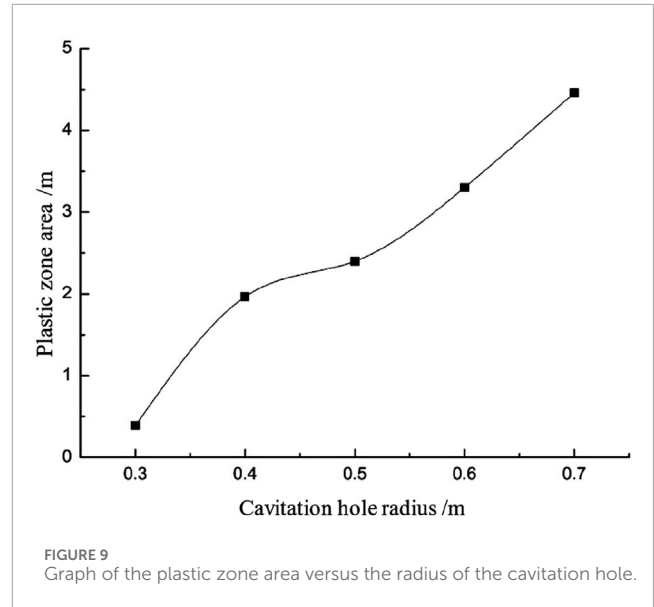
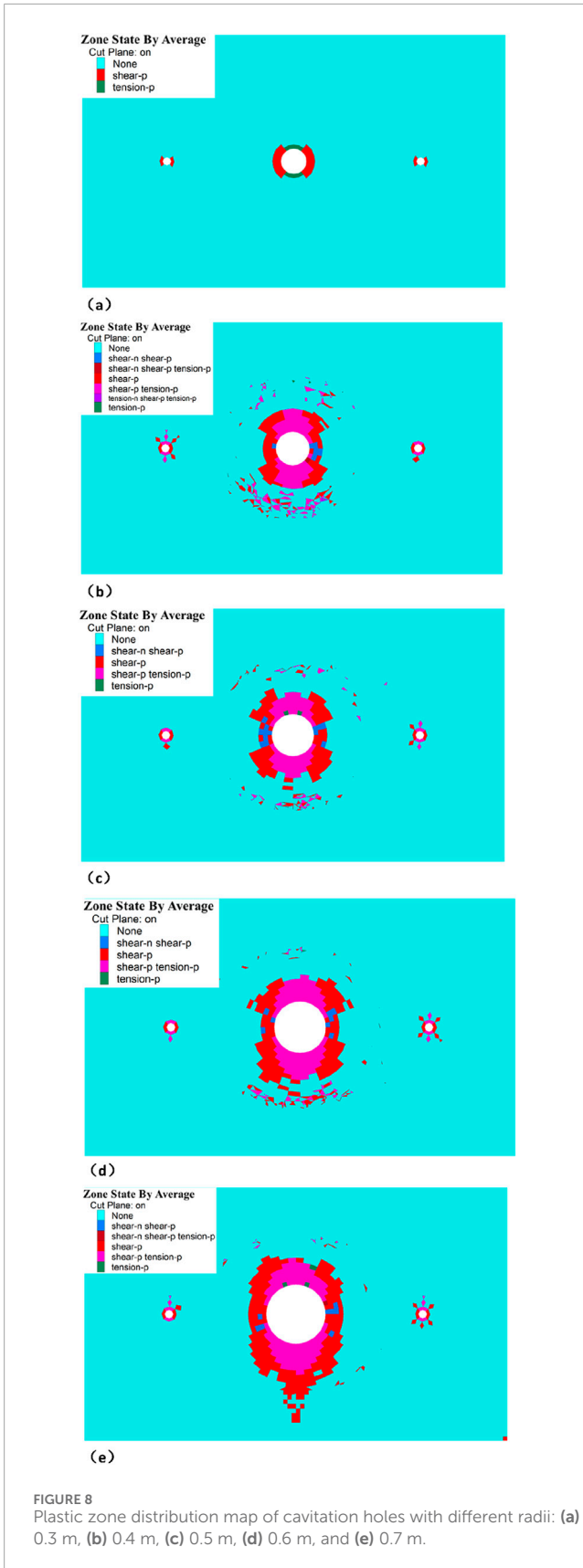
factor for this change is the reconstruction of the tangential stress field: the increase in hole radius breaks the original stress balance around the hole in a wider range, further increases the peak value of tangential stress, and expands its influence radius outward. In the top area, the enhancement of tangential tensile stress not only intensifies the opening degree of existing fractures but also promotes the initiation of new tensile fractures. At the same time, the concentration of tangential compressive stress on the sides causes the interweaving of shear fractures and tensile fractures, forming combined tension–shear failure zones. The increase in the plastic zone near ordinary boreholes is direct evidence of the outward propagation of the tangential stress field generated by the cavitation hole, proving that tangential stress can drive fractures to extend across boreholes and build connected channels for gas flow. At this time, the effect of tangential tensile stress of coal on fracture opening has initially shown advantages, corresponding to the increase of stress-release rate to 56% under this radius, which further verifies the positive correlation between tangential stress, fracture opening, and stress relief.

In Figure 8c, the plastic zones at the haunch, shoulder, top, and bottom of the cavitation hole are significantly expanded compared with those when the radius is 0.4 m, while the plastic zones on both sides remain basically unchanged. This differentiated expansion characteristic is highly consistent with the distribution law of tangential stress: the haunch and shoulder positions are the secondary concentration areas of tangential stress. With the increase in hole radius, the tangential compressive stress in this area further accumulates, leading to the continuous increase of shear stress and extending the depth of shear fractures. Meanwhile, the coverage range of tangential tensile stress at the top and bottom expands, making tensile fractures form longer connected zones.

From the perspective of mechanical mechanism, the gradient change of tangential stress promotes fractures to present a differentiated development mode of “tensile opening at the top, shear extension at the shoulders.” The reason why the plastic zones on both sides are stable is that their tangential stress is in a relatively balanced state without obvious increase or decrease, so the degree of fracture opening does not change significantly. The morphological change of the plastic zone under this radius also provides plastic mechanical support for the subsequent stress-release rate reaching 63%; that is, the expansion of the fracture opening range directly improves the efficiency of coal stress relief.

In Figures 8d,e, the plastic zones at the haunch, shoulder, top, and bottom of the cavitation hole continue to expand, while the plastic zones on both sides still show no obvious changes, and the characteristic of combined tension–shear failure becomes more prominent. This phenomenon indicates that when the cavitation hole radius exceeds 0.5 m, although the peak value of tangential stress continues to increase, the concentrated area of stress distribution does not change, remaining concentrated at the top, bottom, and shoulder positions. At this time, the tangential tensile stress is large enough to not only fully open the primary fractures but also promotes the connection of different fracture zones to form a network fracture system. The continuous action of tangential compressive stress on the sides refines the shear fractures and further improves the degree of coal fragmentation.

The plastic zone area corresponding to the radius of the cavitation hole is extracted, and the change in the plastic zone area is plotted against the radius of the cavitation hole. This is shown in Figure 9, which indicates that the plastic zone area increases gradually with the radius of the cavitation hole. At  $\geq 0.5$  m radius, the increase is approximately linear, indicating that



the radius of the cavitation hole has a significant effect on the plastic zone area.

Based on the plot of the plastic zone area versus the radius of the cavitation hole, two more reasonable fits can be proposed for the curves modeling assumptions (Equations 13–16):

1. Linear model. The model curve is

$$S_{FP1} = a_1R + b_1, \tag{13}$$

where  $a_1$  and  $b_1$  are parameters to be determined in relation to the plastic zone area.

2. 3-function model. The model curve is

$$S_{FP2} = a_2R^3 + b_2R^2 + c_2R + d_2, \tag{14}$$

where  $a_2$ ,  $b_2$ ,  $c_2$ , and  $d_2$  are parameters to be determined in relation to the area of the pressure relief zone.

Based on the extracted values of the radius of the cavitation hole and the plastic zone surface, the fitted curves can be obtained, respectively,

$$S_{FP1} = 9.5R - 2.2, \tag{15}$$

$$S_{FP2} = 116.4R^3 - 177.2R^2 + 95.4R - 15.4. \tag{16}$$

The coefficients of determination of the fit are, respectively,  $R_{FP1}^2 = 0.9636$ ;  $R_{FP2}^2 = 0.9796$ .

The above analysis reveals that the relationship between the plastic zone area of the cavitation hole and the radius of the cavitation hole is better fitted by the cubic function model, and the

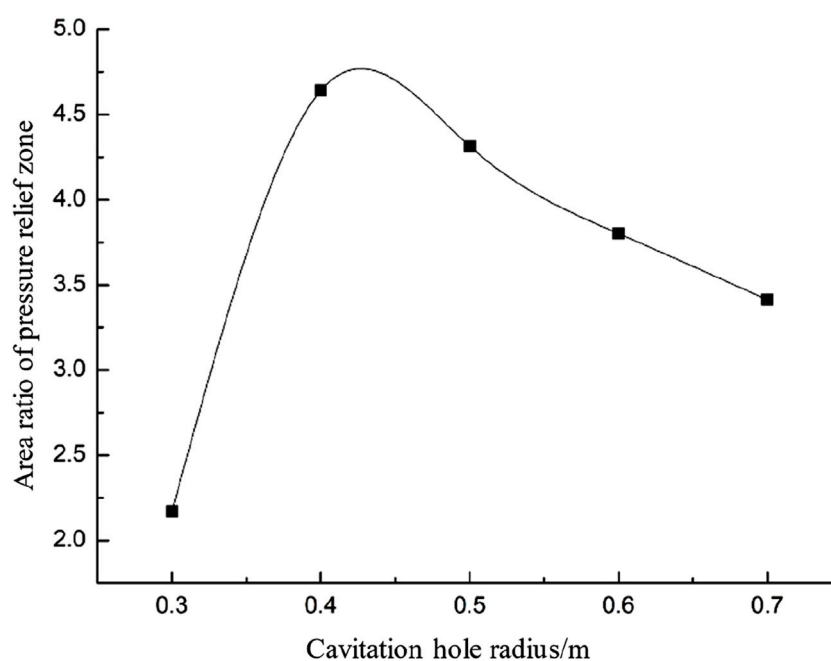


FIGURE 10  
Graph of the variation in the area ratio of the pressure relief zone with the radius of the cavitation hole.

cubic function model can better describe the change of the plastic zone area of the cavitation hole with the radius of the cavitation hole.

### 4.3 Comparison analysis of pressure relief and permeability enhancement effects of cavitation holes with different radii

The above analysis reveals that both the area of the pressure relief zone and the plastic zone area increase with the increase of the radius of the cavitation hole. It shows that the larger the radius of the cavitation hole is, the better the effects of pressure relief and permeability enhancement are. However, in engineering applications, the larger the radius of the cavitation hole, the higher the cost. To understand the relationship between the improved effect of the distressed zone and penetration enhancement and the cost of drilling a larger cavitation hole, we analyzed two aspects of the distressed zone area ratio and the plastic zone area ratio, which are defined in Equation 2 and Equation 3, respectively.

According to Equation 2, pressure relief area ratio was calculated for the corresponding cavitation hole radius and plotted with the cavitation hole radius, as shown in Figure 10, which reveals that the pressure relief area ratio increases and then decreases with the increase of the hole radius, and the maximum value of the pressure relief area ratio is between [0.4, 0.5] m for the hole radius.

The plastic zone area ratios for the corresponding cavitation hole radii are calculated according to Equation 3 and plotted as a function of the variation of hole radius, as shown in Figure 11, which reveals that the area ratio of the plastic zone increases and then decreases with the increase of the radius of the cavitation hole. The maximum value of the area ratio of the plastic zone is at the radius of the

cavitation hole of approximately 0.4 m. The area ratio of the plastic zone increases and then decreases with the increase of the radius of the cavitation hole.

## 5 Engineering applications

The No. 15 coal seam in Baiyangling Coal Mine (Yan, 2022) has an average thickness of 5 m, and the 15108 track drift area is a low-permeability and difficult-to-drain coal seam. The original gas content ranges from 4.52 m<sup>3</sup>/t to 6.5 m<sup>3</sup>/t, the inverse maximum gas pressure is 0.45 MPa, and the maximum initial gas desorption velocity  $\Delta p$  is 38.5 mmHg. The maximum firmness coefficient  $f$  is 1.22, the coal mass failure types are mainly Class III and IV, and the permeability coefficient is 0.079 m<sup>2</sup>/(MPa<sup>2</sup>·d). The cavitation hole radius has a significant impact on drainage effect and borehole stability: when the radius is 0.4 m, the permeability of the plastic zone around the hole reaches 300 times that of the elastic zone, the gas diffusion channel is unobstructed, and the gas pressure around the hole drops below 0.1 MPa after 150 days of drainage. The initial single-hole gas flow rate is nearly twice that of the 0.2 m radius, the stable drainage concentration is 21.49% (with 7 m borehole spacing), which is 3.36 times higher than that of non-cavitation holes (6.39%–8.64%), and the flow attenuation coefficient is 0.015 d<sup>-1</sup>, only 1/4.27 of that of non-cavitation holes (0.118 d<sup>-1</sup>). For the 0.2 m radius, due to the limited plastic zone and insufficient permeability improvement, local high-gas areas still exist after 150 days of drainage. For the 0.6 m radius, the plastic zone doubles, the hole collapse risk is more than three times that of the 0.4 m radius, the borehole spacing must be reduced to 5 m, the construction cost

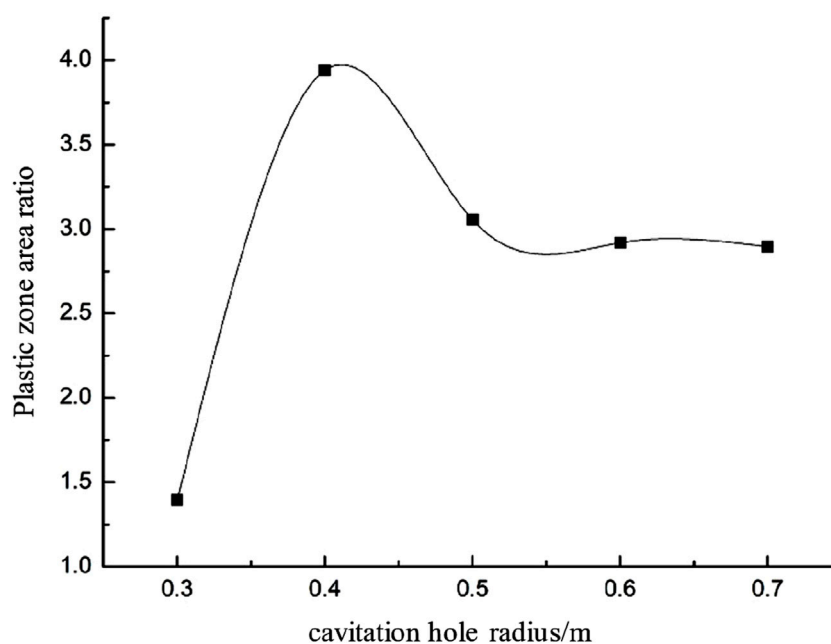


FIGURE 11

Graph of the variation in the plastic zone area ratio with the radius of the cavitation hole. The above analyses show that the optimal cavitation hole radius is between 0.4 m and 0.5 m.

increases by more than 30%, and additional investment in hole collapse control is required.

The optimal parameters are 0.4 m cavitation hole radius + 7 m borehole spacing. At this time, there is no blank zone in the drainage area, and the total drainage volume is 1.41 times higher than that of the 5 m spacing. This practice verifies that when the cavitation hole radius is selected between 0.4 m and 0.5 m, it not only establishes a parameter benchmark for the drainage of low-permeability coal seams but also achieves the dual goals of drainage efficiency and borehole stability. Its applicability has been effectively verified under different coal quality conditions.

## 6 Conclusion

1. Based on the stress distribution characteristics around the cavitation hole, three distinct stress zones are identified: the stress relief area, the stress concentration region, and the original rock stress area. Both the stress relief area and stress concentration region increase gas permeability within the coal mass, while the original rock stress area does not affect coal gas permeability.
2. The area of the stress relief zone and the area of the stress-plastic zone around the cavitation hole vary with the cavitation hole radius according to an exponential function model and a cubic function model, respectively. Their functional models are  $S_{r2} = 1.4 - 15 \times 0.1^R$ ;  $S_{FP2} = 116.4R^3 - 177.2R^2 + 95.4R - 15.4$ .
3. Through FLAC3D numerical simulation and stress distribution mechanism analysis, the optimal cavitation hole radius for achieving peak pressure relief and permeability enhancement lies within the range of 0.4–0.5 m. The scope determined in this study is based on scientific reasoning

and argumentation, which ensures its reliability. Moreover, preliminary validation through numerical calculations supports this conclusion. Subsequent field applications will further verify the scientific nature and effectiveness of this scope.

4. The pressure relief effect of cavitation holes is closely related to the surrounding tangential stress distribution. When the lateral pressure coefficient ( $k < 1$ ), the tangential stress exhibits stress reduction along the B-B line and stress concentration along the A-A line, which correspond to the pressure relief effect and the formation of the plastic zone, respectively. Both effects can be quantified by the pressure relief zone area ratio and the plastic zone area ratio. When the radius of the cavitation hole ranges from 0.4 m to 0.5 m, the tangential stress change achieves the optimal effect, and the relevant indicators of the pressure relief zone and the plastic zone reach their peak values. If the radius is too small, the disturbance to the coal mass will be insufficient; if the radius is too large, the pressure relief efficiency will decrease, and the hole wall is prone to collapse. Meanwhile, the redistribution of tangential stress not only reduces the stress value but also changes the stress state of the coal mass. It promotes gas desorption in the pressure relief zone and unblocks the gas seepage channels in the stress concentration zone, synergistically improving the gas extraction efficiency.

## Data availability statement

The original contributions presented in the study are included in the article/Supplementary Material; further inquiries can be directed to the corresponding author.

## Author contributions

HL: Writing – original draft. JX: Writing – review and editing. ZZ: Writing – review and editing, Data curation. WL: Methodology, Writing – review and editing. YF: Writing – review and editing, Supervision. ZJ: Writing – review and editing.

## Funding

The author(s) declared that financial support was not received for this work and/or its publication.

## Acknowledgements

The authors thank all the athletes for their participation in this study.

## Conflict of interest

Authors HL, ZZ, WL, YF, and ZJ were employed by Zuoquan Wulinhou Mining Co., Ltd.

## References

- Busch, A., and Gensterblum, Y. (2011). CBM and CO<sub>2</sub>-ECBM related sorption processes in coal: a review. *Int. J. Coal Geol.* 87 (2), 49–71. doi:10.1016/j.coal.2011.04.011
- Chen, H., Wang, Z., Chen, X., and Wang, L. (2017). Increasing permeability of coal seams using the phase energy of liquid carbon dioxide. *J. CO<sub>2</sub> Util.* 19, 112–199. doi:10.1016/j.jcou.2017.03.010
- Chen, D., He, W., Xie, S., He, F., Zhang, Q., and Qin, B. (2020). Increased permeability and coal and gas outburst prevention using hydraulic flushing technology with cross-seam borehole. *J. Nat. Gas Sci. Eng.* 73, 103067. doi:10.1016/j.jngse.2019.103067
- Chen, L., Yang, T., Yang, H., and Feng, Z. (2017). Experimental research on timeliness of promoting gas drainage by N<sub>2</sub> injection in coal bed. *J. Northeast. Univ. Nat. Sci.* 38, 26–30. doi:10.12068/j.issn.1005-3026.2017.07.024
- Gao, Y., Lin, B., Yang, W., Li, Z., Pang, Y., and Li, H. (2015). Drilling large diameter cross-measure boreholes to improve gas drainage in highly gassy soft coal seams. *J. Nat. Gas Sci. Eng.* 26, 193–204. doi:10.1016/j.jngse.2015.05.035
- Guo, J., Zhang, H., and Wang, W. (2023). Numerical analysis of the stress-unloading and permeability-increasing characteristics and influencing factors of regional in seam borehole hydraulic cavitation. *Journal Xian University Sci. Technol.* 43 (2), 292–300. doi:10.13800/j.cnki.xakjdx.2023.0209
- He, L., Liu, Y., Shen, K., Yang, X., Ba, Q., and Xiong, W. (2021). Numerical research on the dynamic rock-breaking process of impact drilling with multi-nozzle water jets. *J. Petroleum Sci. Eng.* 207, 109145. doi:10.1016/j.petrol.2021.109145
- Huang, Y., Zheng, P., Fan, N., and Aminian, K. (2014). Optimal scheduling for enhanced coal bed methane production through CO<sub>2</sub> injection. *Appl. Energy* 113, 1475–1483. doi:10.1016/j.apenergy.2013.08.074
- Kong, X., Wang, E., Liu, X., Li, N., Chen, L., Feng, J., et al. (2016). Coupled analysis about multi-factors to the effective influence radius of hydraulic flushing: application of response surface methodology. *J. Nat. Gas Sci. Eng.* 32, 538–548. doi:10.1016/j.jngse.2016.04.043
- Li, D. (2014). Mining thin sub-layer as self-protective coal seam to reduce the danger of coal and gas outburst. *Nat. Hazards* 71 (1), 41–52. doi:10.1007/s11069-013-0898-1
- Li, H., Li, X., Fu, J., Zhu, N., Chen, D., Wang, Y., et al. (2023). Experimental study on compressive behavior and failure characteristics of imitation steel fiber concrete under uniaxial load. *Constr. Build. Mater.* 399, 132599. doi:10.1016/j.conbuildmat.2023.132599
- Li, X., Chen, D., Li, Z., Liu, S., Zhai, M., Li, Y., et al. (2024). Roadway portal and self-moving hydraulic support for rockburst prevention in coal mine and its application. *Phys. Fluids* 36, 124136. doi:10.1063/5.0243798
- Li, X., Cao, Z., and Xu, Y. (2025). Characteristics and trends of coal mine safety development. *Energy Sources, Part A Recovery, Util. Environ. Eff.* 47, 2316–2334. doi:10.1080/15567036.2020.1852339
- Lin, B., Yan, F., Zhu, C., Zhou, Y., Zou, Q., Guo, C., et al. (2015). Cross-borehole hydraulic slotting technique for preventing and controlling coal and gas outbursts during coal roadway excavation. *J. Nat. Gas Sci. Eng.* 26, 518–525. doi:10.1016/j.jngse.2015.06.035
- Liu, Z., and Yu, D. (2012). Elastoplastic stress and displacement analytical solutions to deep-buried circular tunnels considering intermediate principal stress and dilatancy. *Eng. Mech.* 29 (08), 289–296. doi:10.6052/j.issn.1000-4750.2011.08.0511
- Liu, S., Sun, H., Zhang, D., Yang, K., Li, X., Wang, D., et al. (2023). Experimental study of effect of liquid nitrogen cold soaking on coal pore structure and fractal characteristics. *Energy* 275, 127470. doi:10.1016/j.energy.2023.127470
- Liu, S., Li, X., Wang, D., and Zhang, D. (2025). Investigations on the mechanism of the microstructural evolution of different coal ranks under liquid nitrogen cold soaking. *Energy Sources, Part A Recovery, Util. Environ. Eff.* 47 (1), 2595–2612. doi:10.1080/15567036.2020.1841856
- Lou, Z., Wang, K., Kang, M., Zhao, W., Wei, G., Yue, J., et al. (2024). Plugging methods for underground gas extraction boreholes in coal seams: a review of processes, challenges and strategies. *Gas Sci. Eng.* 122, 205225. doi:10.1016/j.jgsce.2024.205225
- Lou, Z., Wang, K., Yao, H., Zhao, W., Qin, H., Wu, Z., et al. (2025). A novel dynamic filling material for plugging fractures around underground gas extraction boreholes: experimental and engineering performances. *Energy* 314, 134202. doi:10.1016/j.energy.2024.134202
- Lu, T., Zhao, Z., and Hu, H. (2011). Improving the gate road development rate and reducing outburst occurrences using the waterjet technique in high gas content outburst-prone soft coal seam. *Int. J. Rock Mech. Min. Sci.* 48 (8), 1271–1282. doi:10.1016/j.ijrmms.2011.09.003
- Lu, Y., Ge, Z., Yang, F., Xia, B., and Tang, J. (2017). Progress on the hydraulic measures for grid slotting and fracking to enhance coal seam permeability. *Int. J. Min. Sci. Technol.* 27 (5), 867–871. doi:10.1016/j.ijmst.2017.07.011
- Ma, K., Yang, T., and Zhao, Y. (2023). Theoretical analysis of water inrush from goaf in floor and mining stability for upward repeated mining. *J. China Coal Soc.* 48, 37–46. doi:10.13225/j.cnki.jccs.2022.0109
- Wang, L., Liao, X., and Chu, P. (2021). Study on mechanism of permeability improvement for gas drainage by cross-seam cavitation borehole. *Coal Sci. Technol.* 49 (5), 75–82. doi:10.13199/j.cnki.cst.2021.05.010

The remaining author(s) declared that this work was conducted in the absence of any commercial or financial relationships that could be construed as a potential conflict of interest.

## Generative AI statement

The author(s) declared that generative AI was not used in the creation of this manuscript.

Any alternative text (alt text) provided alongside figures in this article has been generated by Frontiers with the support of artificial intelligence and reasonable efforts have been made to ensure accuracy, including review by the authors wherever possible. If you identify any issues, please contact us.

## Publisher's note

All claims expressed in this article are solely those of the authors and do not necessarily represent those of their affiliated organizations, or those of the publisher, the editors and the reviewers. Any product that may be evaluated in this article, or claim that may be made by its manufacturer, is not guaranteed or endorsed by the publisher.

- Wang, P., Li, R., and Chen, Z. (2024). Analysis of trapezoid fracture parameters and fracture evolution of overburden in shallow coal seam mining. *J. Henan Polytechnic University(natural Science)* 43 (3), 50–59. doi:10.16186/j.cnki.1673-9787.2023060054
- Xu, Z. (2016). *Elasticity*. 5th edition. Beijing: Higher Education Press.
- Xue, D., Zhou, H., and Tang, X. (2013). Mechanism of deformation-induced damage and gas permeability enhancement of coal under typical mining layouts. *Chin. J. Geotechnical Eng.* 35 (2), 328–336. doi:10.11779/CJGE201302016
- Yan, C. (2022). *Study on technology of increasing flow and promoting pumping of water jet cavitation in parallel drilling along layer*. Henan Polytechnic University. doi:10.13301/j.cnki.ct.2023.01.037
- Yang, X., Wang, G., Du, F., Jin, L., and Gong, H. (2022). N<sub>2</sub> injection to enhance coal seam gas drainage (N<sub>2</sub>-ECGD): insights from underground field trial investigation. *Energy* 239, 122247. doi:10.1016/j.energy.2021.122247
- Zhang, H., Cheng, Y., Liu, Q., Yuan, L., Dong, J., Wang, L., et al. (2017). A novel in-seam borehole hydraulic flushing gas extraction technology in the heading face: enhanced permeability mechanism, gas flow characteristics, and application. *J. Nat. Gas Sci. Eng.* 46, 498–514. doi:10.1016/j.jngse.2017.08.022
- Zhang, H., Cheng, Y., Yuan, L., Wang, L., and Pan, Z. (2019). Hydraulic flushing in soft coal sublayer: gas extraction enhancement mechanism and field application. *Energy Sci. and Eng.* 7 (5), 1970–1973. doi:10.1002/ese3.405
- Zhang, R., Cheng, Y.-P., Yuan, L., Zhou, H., Wang, L., and Zhao, W. (2019). Enhancement of gas drainage efficiency in a special thick coal seam through hydraulic flushing. *Int. J. Rock Mech. Min. Sci.* 124, 104085. doi:10.1016/j.ijrmms.2019.104085
- Zhang, C., Wang, E., Li, B., Kong, X., Xu, J., Peng, S., et al. (2023). Laboratory experiments of CO<sub>2</sub>-enhanced coalbed methane recovery considering CO<sub>2</sub> sequestration in a coal seam. *Energy* 262, 125473. doi:10.1016/j.energy.2022.125473
- Zhou, A., Zhang, M., Wang, K., Elsworth, D., Wang, J., and Fan, L. (2020). Airflow disturbance induced by coal mine outburst shock waves: a case study of a gas outburst disaster in China. *Int. J. Rock Mech. Min. Sci.* 128, 104262. doi:10.1016/j.ijrmms.2020.104262
- Zhou, L., Zhou, X., Bai, G., Li, X., and Luo, M. (2023). Effect of damage zone around borehole on carbon dioxide injection promoted gas extraction in soft and low-permeability coal seam. *Front. Earth Sci.* 17 (3), 776–787. doi:10.1007/s11707-022-1036-8